DEUTSCHES ELEKTRONEN-SYNCHROTRON DESY

DESY 88-030
March 1988

CAUSTICS IN A CUBIC SU(2) LATTICE MODEL WITH ANTI-PERIODIC BOUNDARY CONDITIONS

by

B. Raabe

II. Institut für Theoretische Physik, Universität Hamburg

ISSN 0418-9833

NOTKESTRASSE 85 · 2 HAMBURG 52

To be sure that your preprints are promptly included in the
HIGH ENERGY PHYSICS INDEX ,
send them to the following address (if possible by air mail) :

DESY
Bibliothek
Notkestrasse 85
2 Hamburg 52
Germany

DESY 88-030
March 1988

ISSN 0418-9833

Caustics in a Cubic $SU(2)$ Lattice Model with Anti-periodic Boundary Conditions

by

B. Raabe*

II.Institut für Theoretische Physik, Universität Hamburg

Abstract

In order to investigate the weak coupling limit of lattice gauge theories it has been suggested recently to apply the semiclassical approximation to the Schrödinger equation in the Hamiltonian formalism. This method is used to study pure $SU(2)$ gauge theory on a cube with sides of length one lattice constant and with anti-periodic boundary conditions. We show the existence of caustics, i.e. envelopes of families of classical trajectories where the ground state wave function peaks, and describe their shape.

* Supported in part by BMFT and by Doktorandenstipendium der Stadt Hamburg

Introduction

In their article on 'Caustics in a Simple $SU(2)$ Lattice Gauge Theory Model' [1] Bartels and Wu considered pure $SU(2)$ in the Hamiltonian formalism of Kogut and Susskind [2]. The dependence of the Hamiltonian operator[1]

$$H = \frac{g^2}{2} T + \frac{2}{g^2} V \tag{1}$$

on the coupling constant g^2 which becomes small in the continuum limit (see e.g. [3, ch. 12]) led them to apply the semiclassical approximation in analogy with the usual short wave asymptotics [4, app. 11] known from quantum mechanics (WKBJ approximation) and optics (eikonal approximation). Substituting the ansatz

$$\Psi = A e^{\frac{1}{g^2} S} \tag{2}$$

into the Schrödinger equation with Hamiltonian (1) one obtains the Hamilton-Jacobi equation and from it the equations of motion of a mechanical system with many degrees of freedom. In order to analyse the ground state of (1) Bartels and Wu examined the resulting classical trajectories for the gauge field on one and two plaquettes with free boundary conditions. As the classically allowed region consists only of an isolated point, the origin, the trajectories of interest which leave in all possible directions of configuration space have zero energy and their action $S = i\overline{S}$ is purely imaginary. At large distances the wave function

$$\Psi = A e^{-\frac{1}{g^2} \overline{S}} \tag{3}$$

is therefore suppressed. But at intermediate distances regions exist where neighbouring trajectories intersect. On these focal surfaces or caustics the prefactor A which represents fluctuations around the classical paths and can also be interpreted as the square root of their density [5, ch. 11-18] grows large and competes the exponential decay. In the limit $g^2 \to 0$ A behaves like $const. \cdot g^{-p}$ where the positive fractional power p depends on the shape of the caustic and may be inferred by transforming it to its normal form (cp. [1, sect. 4.2-4.3]; for the general theory see [4, app. 12] or [6]). This enhancement of the ground state wave function on the caustics may yield a significant contribution to physical observables.

The goal of this article is to extend these studies to another simple model, namely pure $SU(2)$ on a cube with anti-periodic boundary conditions. Whereas for a cube with free boundary conditions the Hamiltonian depends on five $SU(2)$ group elements after gauge fixing on the maximal tree [7] and a cube with periodic boundary conditions still depends on nine parameters (cp. [8]) this model has essentially only three degrees of freedom and is therefore comparable in complexity with the two-plaquette model. We show that it also has caustics which strongly resemble those of the two-plaquette model, but are a little closer to the origin. Due to the more complex potential with four inequivalent minima they show a much richer structure which may be interpreted as a first hint at a self-repetitive pattern.

In the first part of this report we briefly collect the necessary definitions of the Hamiltonian lattice formalism, introduce the model under investigation and derive the equations of motion

[1] T is the electric part and plays the role of kinetic energy, whereas the magnetic part V provides the potential.

after gauge fixing. In the second part the result of the numerical analysis, the shape of the caustic formed by the first and second focal points, is presented and compared with the findings of Bartels and Wu for the two-plaquette model.

Hamiltonian Operator and Equations of Motion

For a lattice gauge theory with arbitrary continuous gauge group G the electric and magnetic parts of the Hamiltonian (1) are given by [3, ch. 15]

$$\begin{aligned} T &= \frac{1}{a}\sum_{K\subset\Lambda} J^2(g_K) \\ \text{and} \qquad V &= \frac{1}{a}\sum_{P\subset\Lambda}(\mathrm{Re}(\mathrm{Tr}(1-g_{\partial P}))). \end{aligned} \tag{4}$$

The lattice constant a will be set equal to one in the sequel. The sum in V extends over all plaquettes P of the lattice Λ and $g_{\partial P}$ is the product of the group elements on the links surrounding P, whereas the sum in T extends over all links K in Λ, g_K is the gauge field on link K and J^2 the quadratic Casimir operator of G which is realised as a differential operator in the group parameters. Let

$$g = e^{\sum \vartheta^a \lambda_a} \in \mathrm{G} \tag{5}$$

be an arbitrary element of the gauge group with the generators λ_a in the algebra of G normalised according to

$$\mathrm{Tr}(\lambda_a \lambda_b) = \delta_{ab}; \tag{6}$$

the metric tensor of the group at g is then given by

$$M_{ab}(g) = c\,\mathrm{Tr}((g^{-1}\frac{\partial}{\partial\vartheta^a}g)(g^{-1}\frac{\partial}{\partial\vartheta^b}g)). \tag{7}$$

This definition is unique up to the positive multiplicative constant c (for further information see [9, sect. II and app. A] and references cited therein). The Casimir operator J^2 is identical to the corresponding Laplace-Beltrami operator except for its sign.

$$-J^2(g) = \Delta(g) = M(g)^{-\frac{1}{2}}\frac{\partial}{\partial\vartheta^a}M(g)^{\frac{1}{2}}((M^{-1})^{ab}(g))\frac{\partial}{\partial\vartheta^b} \tag{8}$$

where $M(g) = \det(M_{ab}(g))$ and $(M^{-1})^{ab}(g)$ is the inverse metric tensor.

The group $SU(2)$ we are concerned with as well as its algebra can be represented by the Pauli

matrices and therefore each element $g \in SU(2)$ may be written as

$$g = \exp(i\sum_{a=1}^{3} x^a\sigma_a) = y^0\cdot\mathbf{1} + i\sum_{a=1}^{3} y^a\sigma_a$$

$$\text{with} \qquad y^0 = \cos x^0, \qquad x^0 = (\sum_{a=1}^{3}(x^a)^2)^{\frac{1}{2}} \le \pi, \tag{5'}$$

$$y^i = \begin{cases} \dfrac{x^i}{x^0}\sin x^0 & \text{for} \quad x^0 \neq 0 \\ 0 & \text{otherwise} \end{cases}, \qquad \sum_{a=0}^{3}(y^a)^2 = 1.$$

As $SU(2)$ is isomorphic to the three-dimensional sphere $S^3 \subset R^4$ it can also be parametrised by the angles Θ, ϑ and φ which are related to the y^a via

$$\begin{aligned} y^0 &= \cos\Theta \\ y^1 &= \sin\Theta\sin\vartheta\cos\varphi \\ y^2 &= \sin\Theta\sin\vartheta\sin\varphi \\ y^3 &= \sin\Theta\cos\vartheta. \end{aligned} \tag{9}$$

Because the generators now obey

$$\mathrm{Tr}(i\sigma_a\, i\sigma_b) = -2\delta_{ab} \tag{6'}$$

we have to scale the metric tensor and do so in agreement with references [1] and [8] to obtain

$$M^{SU(2)}{}_{ab}(g(\Theta,\vartheta,\varphi)) = 4\begin{pmatrix} 1 & & \\ & \sin^2\Theta & \\ & & \sin^2\Theta\sin^2\vartheta \end{pmatrix}. \tag{7'}$$

The Laplacian reads

$$\Delta^{SU(2)}(g(\Theta,\vartheta,\varphi)) = \frac{1}{4}\{\frac{\partial^2}{\partial\Theta^2} - 2\cot\Theta\frac{\partial}{\partial\Theta} - \frac{\ell^2(g)}{\sin^2\Theta}\} \tag{8'}$$

with

$$-\ell^2(g(\Theta,\vartheta,\varphi)) = \frac{1}{\sin\vartheta}\frac{\partial}{\partial\theta}(\sin\vartheta\frac{\partial}{\partial\vartheta}) + \frac{1}{\sin^2\vartheta}\frac{\partial^2}{\partial\varphi^2}.$$

After the semiclassical approximation has been investigated for pure $SU(2)$ on one and two plaquettes with free boundary conditions in [1] one wishes to employ this method to larger lattices. A model comparabel in complexity with the two-plaquette case results if one imposes anti-periodic boundary conditions on the gauge fields on a cube (see fig. 1). Let $g(m,n) = g(n,m)^{-1} = g(n,m)^{\dagger} \in SU(2)$ be the gauge field on the directed link connecting point m with point n: we then require

$$\begin{aligned} & g(1,2) = g(3,4) = g(5,6) = g(7,8) \equiv k(1), \\ & g(1,4) = g(3,2) = g(5,8) = g(7,6) \equiv k(2) \\ \text{and} \qquad & g(1,6) = g(3,8) = g(5,2) = g(7,4) \equiv k(3). \end{aligned} \tag{10}$$

The anti-periodicity of the $g(m,n)$ implies that only two of the eight gauge transformations

$$g(m,n) \to h(m)\,g(m,n)\,h(n)^{-1}, \quad h(i) \in SU(2), \tag{11}$$

in the corners of the cube are independent. The notation has been chosen in such a way that a transformation by $h \in SU(2)$ at the origin (corner no. 1) implies the same transformation in all odd-numbered corners (and analogously for the even-numbered ones). This gauge freedom can be used to simplify the Hamiltonian

$$\begin{aligned} H = \quad & \frac{g^2}{2}\,4\sum_{i=1}^{3} J^2(k(i)) \\ & + \frac{2}{g^2}\,2\,\{6 - \mathrm{Tr}((k(1)k(3)^\dagger)^2) \\ & \qquad - \mathrm{Tr}((k(3)k(2)^\dagger)^2) - \mathrm{Tr}\{(k(2)k(1)^\dagger)^2)\}. \end{aligned} \tag{12}$$

Fixing the gauge on the maximal tree of the lattice, viz. setting $k(3) \equiv 1$, and choosing

$$\ell(1) = k(1)k(3)^\dagger \quad \text{and} \quad \ell(2) = k(3)k(2)^\dagger \tag{13}$$

as new variables, the procedure described by Bronzan [7] results in

$$\begin{aligned} H = \quad & \frac{g^2}{2}\,4\cdot 2\{\vec{J}_R^{\,2}(\ell(1)) + \vec{J}_L^{\,2}(\ell(2)) - \vec{J}_R(\ell(1))\vec{J}_L(\ell(2))\} \\ & + \frac{2}{g^2}\,2\,\{6 - \mathrm{Tr}(\ell(1)^2) - \mathrm{Tr}(\ell(2)^2) - \mathrm{Tr}((\ell(1)\ell(2))^2)\}, \end{aligned} \tag{14}$$

where

$$\vec{J}_{\substack{L\\R}}(g(\vec{x})) = \mp\frac{1}{2}(\vec{\ell} + x^0\vec{p}) \tag{15}$$

with $\vec{\ell} = \vec{x} \times \vec{p}$ and $\vec{p} = -i\vec{\nabla}$ as well as $\vec{J}_L^{\,2} = \vec{J}_R^{\,2} = J^2$. The $\vec{J}_{\substack{L\\R}}(g(\Theta,\vartheta,\varphi))$ are given in [1] . But the Hamiltonian (14) is still invariant under a 'global' transformation of the loop variables

$$\ell(i) \to s\,\ell(i)\,s^{-1}, \quad s \in SU(2). \tag{16}$$

As the gauge invariant ground state wave function Ψ can only depend on the relative angle $\vartheta_r = \vartheta(2) - \vartheta(1)$ between the $l(i)$ and is invariant under rotations of them around each other only three of the six angle-variables in $l(1)$ and $l(2)$ are relevant, namely

$$\Theta_1 \equiv \Theta(1), \quad \Theta_2 \equiv \Theta(2) \quad \text{and} \quad \vartheta_r \equiv \vartheta(1) - \vartheta(2) \tag{17}$$

(cp. [1, sect. 4.1]). The ansatz $\Psi = Ae^{\frac{i}{g^2}S}$ together with $p_\alpha = \partial_\alpha S$ now leeds to the semiclassical Hamiltonian function and the corresponding equations of motion. But in the limit $g^2 \to 0$ the classically allowed region shrinks to those points where the potential is minimal and the trajectories of interest all lie in the forbidden region ($V > E$) as can be seen by multiplying the Schrödinger equation by g^2. We therefore make the ansatz $\overline{\Psi} = \overline{A}\,e^{-\frac{1}{g^2}\overline{S}}$ instead. As $\overline{S} = -iS$, the momenta

$$\overline{p} = \frac{\partial\overline{S}}{\partial x} = -i\frac{\partial S}{\partial x} = -ip \tag{18}$$

and also the time $\bar{t} = it$ are purely imaginary. The resulting equations of motion for x, $\overline{p}$ and $\bar{t}$

$$\frac{dx}{d\bar{t}} = -\frac{\partial H}{\partial\overline{p}}, \quad \frac{d\overline{p}}{d\bar{t}} = \frac{\partial H}{\partial x}, \tag{19}$$

where

$$H = H(x,p,t) = H(x, i\overline{p}, -i\bar{t}), \tag{20}$$

are formally equivalent with the canonical equations

$$\frac{dx}{d\bar{t}} = \frac{\partial\overline{H}}{\partial\overline{p}}, \quad \frac{d\overline{p}}{d\bar{t}} = -\frac{\partial\overline{H}}{\partial x} \tag{21}$$

of a Hamiltonian function

$$\overline{H}(x,\overline{p},t) = -H(x, i\overline{p}, -i\bar{t}) = T(x,\overline{p},\bar{t}) - V(x). \tag{22}$$

In other words, imaginary time can be avoided by reversing the sign of the potential. When computing the equations of motion we furthermore used that

$$\mathrm{Tr}((\ell(1)\ell(2))^2) = 4(\cos\Theta_1\cos\Theta_2 - \cos\vartheta_r\sin\Theta_1\sin\Theta_2)^2 - 2, \tag{23}$$

and the potential can therefore be written as

$$\begin{aligned} V = \; & 8\,\{3 - \cos^2\Theta_1 - \cos^2\Theta_2 \\ & - (\cos\Theta_1\cos\Theta_2 - \cos\vartheta_r\sin\Theta_1\sin\Theta_2)^2\} \end{aligned} \tag{24}$$

In fig. 2 it is shown in sections of different ϑ_r. In contrast to the potential in the two-plaquette model [1] it has four gauge in-equivalent minima. Apart from the obvious symmetry of the total Hamiltonian under exchange of Θ_1 and Θ_2 it is also invariant under

$$\Theta_1 \to \pi - \Theta_1, \quad \Theta_2 \to \Theta_2, \quad \vartheta_r \to \pi - \vartheta_r. \tag{25}$$

From the Hamiltonian function with the potential turned around which for simplicity is again denoted by H,

$$\begin{aligned} H = \frac{1}{g^2}\{ \; & p_{\Theta_1}^2 + \frac{1}{\sin^2\Theta_1}p_{\vartheta_r}^2 \\ & + p_{\Theta_2}^2 + \frac{1}{\sin^2\Theta_2}p_{\vartheta_r}^2 \\ & - \cos\vartheta_r p_{\Theta_1}p_{\Theta_2} + (\cot\Theta_1\cot\Theta_2\cos\vartheta_r - 1){p_{\vartheta_r}}^2 \\ & + \sin\vartheta_r p_{\vartheta_r}(\cot\Theta_2 p_{\Theta_1} + \cot\Theta_1 p_{\Theta_2})\} \\ & - \frac{16}{g^2}\{3 - \cos^2\Theta_1 - \cos^2\Theta_2 \\ & - (\cos\Theta_1\cos\Theta_2 - \cos\vartheta_r\sin\Theta_1\sin\Theta_2)^2\}, \end{aligned} \tag{26}$$

one obtains the equations of motion of the angles

$$\begin{aligned} \dot{\Theta}_1 &= 2\,p_{\Theta_1} - \cos\vartheta_r p_{\Theta_2} + \sin\vartheta_r\cot\Theta_2\,p_{\vartheta_r}, \\ \dot{\Theta}_2 &= 2\,p_{\Theta_2} - \cos\vartheta_r p_{\Theta_1} + \sin\vartheta_r\cot\Theta_1\,p_{\vartheta_r}, \\ \dot{\vartheta}_r &= 2\,(\frac{1}{\sin^2\Theta_1} + \frac{1}{\sin^2\Theta_2} + \cos\vartheta_r\cot\Theta_2\cot\Theta_1 - 1)\,p_{\vartheta_r} \\ & \quad + \sin\vartheta_r(\cot\Theta_2 p_{\Theta_1} + \cot\Theta_1 p_{\Theta_2}), \end{aligned} \tag{27.a}$$

and their canonical momenta

$$\begin{aligned}
\dot{p}_{\Theta_1} &= \frac{1}{\sin^2\Theta_1}\{(2\cot\Theta_1 + \cos\vartheta_r\cot\Theta_2){p_\vartheta}^2 - \sin\vartheta_r p_\vartheta p_{\Theta_2}\} \\
&\quad + 32\{\sin\Theta_1\cos\Theta_1 + (\cos\Theta_1\cos\Theta_2 - \cos\vartheta_r\sin\Theta_2\sin\Theta_1)\cdot \\
&\qquad \cdot(\sin\Theta_1\cos\Theta_2 + \cos\vartheta_r\cos\Theta_1\sin\Theta_2)\}, \\
\dot{p}_{\Theta_2} &= \frac{1}{\sin^2\Theta_2}\{(2\cot\Theta_2 - \cos\vartheta_r\cot\Theta_1){p_\vartheta}^2 - \sin\vartheta_r p_\vartheta p_{\Theta_1}\} \\
&\quad + 32\{\sin\Theta_2\cos\Theta_2 + (\cos\Theta_1\cos\Theta_2 - \cos\vartheta_r\sin\Theta_1\sin\Theta_2)\cdot \\
&\qquad \cdot(\cos\Theta_1\sin\Theta_2 + \cos\vartheta_r\sin\Theta_1\cos\Theta_2)\}, \\
\dot{p}_{\vartheta_r} &= \sin\vartheta_r\{\cot\Theta_1\cot\Theta_2{p_\vartheta}^2 - p_{\Theta_1}p_{\Theta_2}\} \\
&\quad - \cos\vartheta_r\{\cot\Theta_1 p_{\Theta_2} + \cot\Theta_2 p_{\Theta_1}\}p_\vartheta \\
&\quad - 32\sin\vartheta_r\sin\Theta_1\sin\Theta_2\{\cos\Theta_1\cos\Theta_2 - \cos\vartheta_r\sin\Theta_1\sin\Theta_2\},
\end{aligned} \tag{27.b}$$

where the overall factor of g^2 has been dropped.

The caustics consist of focal points, i.e. points of intersection of trajectories infinitesimally close to each other. Let

$$x(t) = (\Theta_1(t),\ \Theta_2(t),\ \vartheta_r(t)) \tag{28}$$

be a trajectory and

$$\begin{aligned}
x(t) + \delta^l x(t) &= (\Theta_1(t) + \delta^l\Theta_1(t),\ \Theta_2(t) + \delta^l\Theta_2(t),\ \vartheta_r(t) + \delta^l\vartheta_r(t)), \\
l &= 1 \text{ or } 2
\end{aligned} \tag{29}$$

two neighbouring ones with the $\delta^l x$ infinitesimal. For times not too large the deviations $\delta^l x$ will stay small. A focal point is reached when the volume of the parallelepiped spanned by $\dot{x}$, $\delta^1 x(t)$ and $\delta^2 x(t)$ vanishes, i.e. when

$$\det\begin{pmatrix} \dot{\Theta}_1 & \delta^1\Theta_1 & \delta^2\Theta_1 \\ \dot{\Theta}_2 & \delta^1\Theta_2 & \delta^2\Theta_2 \\ \dot{\vartheta}_r & \delta^1\vartheta_r & \delta^2\vartheta_r \end{pmatrix} = 0 \tag{30}$$

(cp. also fig. 3). To determine the shape of the caustics one therefore has to solve the equations of motion (27) for three neighbouring trajectories and compute the determinant (30). Instead of searching for an analytic solution – an obviously rather hopeless task – the integration was performed numerically on a computer using the well-known Runge-Kutta procedure (cp. e.g. [10]) for the reference trajectory (28) and the less consumptive Euler-Cauchy procedure [10] for the small deviations $\delta^l x$ (29) and a linearised version of equations (20) which we do not reproduce. These were derived with the help of REDUCE, a program designed for algebraic manipulations, and will not be reproduced here.

To fix the starting values for the momenta the quadratic approximation of the Hamiltonian operator

$$H_Q = \frac{g^2}{2}T_Q + \frac{2}{g^2}V_Q \tag{31}$$

can be used. The substitution

$$\vec{x}_{1,2} = \frac{\sqrt{2}}{2}(\vec{z}_1 \mp \vec{z}_2), \tag{32}$$

diagonalises the potential

$$V_Q = 16(\vec{x}_1^2 + \vec{x}_2^2 + \vec{x}_1\cdot\vec{x}_2) = 8(3\vec{z}_1^2 + \vec{z}_2^2) \tag{33}$$

and the kinetic energy

$$T_Q = -2(\Delta_{\vec{x}_1} - \Delta_{\vec{x}_2} \quad \nabla_{\vec{x}_1}\cdot\nabla_{\vec{x}_2}) = -(\Delta_{\vec{z}_1} + 3\Delta_{\vec{z}_2}). \tag{34}$$

where

$$\Delta_{\vec{x}} = {\nabla_{\vec{x}}}^2, \quad \nabla_{\vec{x}} = \left(\frac{\partial}{\partial x_1}, \frac{\partial}{\partial x_2}, \frac{\partial}{\partial x_3}\right). \tag{35}$$

For $E = 0$ one obtains

$$S = 4\sqrt{\frac{2}{3}}(\vec{x}_1^2 + \vec{x}_2^2 - \vec{x}_1\cdot\vec{x}_2), \tag{36}$$

and hence

$$\begin{aligned}
p_{\Theta_{1,2},\text{start}} &= 4\sqrt{\frac{2}{3}}(2\Theta_{2,1} - \cos\vartheta_r\Theta_{1,2}) \\
p_{\vartheta_r,\text{start}} &= -4\sqrt{\frac{2}{3}}\sin\vartheta_r\Theta_1\Theta_2
\end{aligned} \tag{37}$$

The following section describes the results of the numerical analysis.

The Shape of the Caustic

As outlined in the last section we traced the trajectories of the semiclassical approximation and determined their first and second focal points. To begin with, a rough panoramic view of the position of the caustics will be given. In a second step we shall describe their shape in more detail and compare it with the two-plaquette model (or TPM for short) investigated by Bartels and Wu [1]. Finally, we shall go into detail about the rich fine structure of the caustic.

As derived above the configuration space of the semiclassical trajectories is three-dimensional in the cube model (CM) and parametrised by the angles Θ_1, Θ_2 and ϑ_r as in the TPM. Because of the symmetry under exchange of Θ_1 and Θ_2 we shall also use the coordinates

$$\begin{aligned}
\Theta_\Sigma &= \frac{1}{2}(\Theta_1 + \Theta_2) \\
\text{and} \qquad \Theta_\Delta &= \frac{1}{2}(\Theta_2 - \Theta_1).
\end{aligned} \tag{38}$$

When following the trajectories one finds the first two focal points in a relatively small region Γ (see fig. 4) which is centered around the point $(\Theta_\Sigma = \frac{7}{10}\pi;\ \Theta_\Delta = 0;\ \vartheta_r = \frac{\pi}{20})$. For the third

and fourth focal point there is a similar region of accumulation Γ' around ($\Theta_\Sigma = \frac{7}{40}\pi$; $\Theta_\Delta = 0$; $\vartheta_r = \frac{2}{3}\pi$) although it is not localised as precisely as Γ. This has to be attributed not least to numerical inaccuracies in the determination of the positions of the focal points. It should be comparable to the size of a single step of our integration procedure and therefore not exceed $\pm 0.001\,\pi$ at the first focal point but of course increases with time. These deviations from the true positions should at most result in a deformation and displacement of actual caustics but not lead to fake focal surfaces. This view is supported by singularity theory: As all the caustics encountered are 'generic' or 'in general position' they are stable and their shape is preserved under small perturbations (for a rigorous formulation of this statement see e.g. [6]).

The caustic in the region Γ looks by and large the same as that of the TPM (s. fig. 5 which is almost identical with fig. 8 in [1]). There is a line in the CM resembling the fold singularity (= Whitney's tuck = cusp) given by the line joining A, B and C in fig. 5 as well as a point corresponding to the bottle neck F (= hyperbolic umbilic). These focal surfaces are Lagrangean singularities, i.e. singularities of the projection map of the six-dimensional phase space to the three-dimensional configuration space. In the classification given by Arnold et al. [6] the cusp is called A_3, the bottle neck D_4^+ and the surfaces connecting them A_2 (for a brief introduction see [4, app. 12]). The normal forms of these caustics were used in [1] to construct the ground state wave function in the vicinity of the caustics. All singularities in the CM are also of types A_2, A_3 and D_4^+. The position of the caustic here is closer to the origin and the ($\vartheta_r = 0$)-plane than in the TPM as has been conjectured for larger lattice models by Bartels and Wu. The fold ABC intersects the plane of symmetry ($\Theta_\Delta = 0$) and the ($\vartheta_r = 0$)-plane at

$$\begin{aligned} & \Theta_\Sigma(B) \simeq 0.76\pi \simeq 2.39 && \text{in the TPM} \\ \text{whereas} \quad & \Theta_\Sigma(B) \simeq 0.66\pi \simeq 2.07 && \text{in the CM} \end{aligned}$$

and the value of ϑ_r in F is given by

$$\begin{aligned} & \vartheta_r(F) \simeq 0.53\pi \simeq 1.66 && \text{in the TPM} \\ \text{and by} \quad & \vartheta_r(F) \simeq 0.07\pi \simeq 0.22 && \text{in the CM.} \end{aligned}$$

The position of the point F shows clearly that the caustic in the CM is compressed to about one seventh its size in the TPM. We therefore presume an even stronger peak of the ground state wave function in this region in the CM than in the TPM.

Up to now the similarities of the caustics in the CM and the TPM have been stressed. There are however striking differences which even conceal the parallels at first sight. We shall describe them separately for the upper (with respect to fig. 5, $\vartheta_r > \vartheta_r(F) \simeq -0.07\pi$) and the lower ($\vartheta_r < \vartheta_r(F)$) part. Because of the ($\Theta_1 \leftrightarrow \Theta_2$)-symmetry it is sufficient to regard only one half of the cube, e.g. that with $\Theta_\Delta > 0$. In the TPM one thus obtains the picture shown in fig. 6 for the upper part where for ease of visualisation not only the edge of the caustic Σ_{TPM} but also some lines of intersection with planes of constant Θ_Δ are drawn. In the CM on the other hand the part of the caustic aiming at C ($\Theta_1 = 0, \Theta_2 = \pi$ or equivalently $\Theta_\Sigma = \Theta_\Delta = \frac{\pi}{2}$) is twisted (cp. fig. 7). But this is still not the full shape for the line joining the points B and C is placed slightly above the ($\vartheta_r = 0$)-plane and is joined to it by a seam BB'C (cp. fig. 8). Fig. 9 shows a detail of this upper part viewed along the Θ_2-axis under an angle of 45° from above. The pattern consisting of the hyperbolic umbilic F, the sharp edge

FD in the plane of symmetry, the seam BB'C and the twist is depicted in fig. 9.a whereas fig. 9.b shows a net of focal points lying on Σ_{CM}. Fig. 10 demonstrates the formation of the seam in the ($\Theta_\Delta = 0$)-plane. Fig. 10.a gives not the focal points but the semiclassical trajectories themselves. The part of Σ_{CM} which originates from them is just the envelope of these curves (fig. 10.b).

To determine the exact position of the point B' in the plane of symmetry given by $\Theta_\Delta = 0$ we have to follow trajectories close to the axis $\Theta_\Delta = \vartheta_r = 0$ and find the point of intersection with it. Their linearised equations of motion read

$$\begin{aligned} \dot{\Theta}_\Sigma &= p_{\Theta_\Sigma} \\ \dot{p}_{\Theta_\Sigma} &= 32(\frac{1}{2} + \cos 2\Theta_\Sigma)\sin\Theta_\Sigma \end{aligned} \tag{39.a}$$

and

$$\begin{aligned} \dot{\vartheta}_r &= 2(3\cot^2\Theta_\Sigma + 1)p_{\vartheta_r} + 2\cot\Theta_\Sigma\, p_{\Theta_\Sigma}\,\vartheta_r \\ \dot{p}_{\vartheta_r} &= -({p_{\Theta_\Sigma}}^2 + 32\sin^2\Theta_\Sigma\cos 2\Theta_\Sigma)\,\vartheta_r - 2\cot\Theta_\Sigma\, p_{\Theta_\Sigma}\, p_{\vartheta_r}. \end{aligned} \tag{39.b}$$

With

$$\Theta_\Sigma(t) = \operatorname{arccot}(\frac{\sqrt{3}}{3}\sinh(-4\sqrt{6}t + \text{const.})) \tag{40}$$

solving (39.a) for the boundary conditions

$$\lim_{t\to-\infty}\Theta_\Sigma(t) = \lim_{t\to-\infty} p_{\Theta_\Sigma}(t) = 0, \tag{41}$$

the problem reduces to the determination of the first zero of $\vartheta_r(t)$ in equations (39.b) which can be cast into the form

$$(x^2+1)(x^2+3)\frac{d^2\vartheta_r}{dx^2} - x(x^2+3)\frac{d\vartheta_r}{dx} + 2\vartheta_r = 0 \tag{42}$$

where $x = \sinh(-4\sqrt{6}t)$. Thus already in this approximation to the full equations (27) an analytic solution is hard to obtain. The numerical results agree with those for the full equations (Θ_Σ (B') = $0.666\,\pi$).

Fig. 11 displays one half of the lower part of Σ_{CM}. Since the lateral faces of the (Θ_1, Θ_2, ϑ_r)-cube, that is to say the ($\Theta_1 = 0$)-, ($\Theta_1 = \pi$)-, ($\Theta_2 = 0$)- and ($\Theta_2 = \pi$)-planes, should be contracted into lines, because e.g. group elements in the ($\Theta_1 = 0$)-plane with the same Θ_2 but different ϑ_r are actually identical, the points C in figs. 6-8 and T in fig. 11 have to be identified. Thus it does not come as a surprise to see that part of the lower half of Σ_{CM} pointing at T=C approach the equivalent part of the upper half. But not only T and the symmetrical point R (cp. fig. 5) but the whole line RST is 'lifted' to larger values of ϑ_r than shown in fig. 11. As the point U of the TPM corresponds to U' in the CM which is no longer in the corner of the cube but at $\Theta_\Sigma \simeq 0.74\pi \simeq 2.34$, $\vartheta_r = 0$, the lower part of Σ_{CM} as a whole looks like a triangular bowl (RTU') in the middle of which a mountain with summit F rises (cp. fig. 12). This bowl is not smooth however, but has a ridge FU' (just as the line FD in the upper half of Σ_{CM}) because the line TU' intersects the plane of symmetry with non-zero angle. Fig. 13 displays the projection of half of the lower part of Σ_{CM} onto the plane of symmetry in its structure (fig. 13.a) as well as with the help of a net of focal points

(fig. 13.b). In fig. 14 we have tried to put things together and draw half of the upper and lower part in one picture.

This still does not completely finish the analysis of the caustic Σ_{CM} constituted by the first and second focal points. For trajectories with a starting value of $\vartheta_{r,\mathrm{start}} \geq 0.9\pi$ which get closer and closer to the corners of the cube the amount of computer time needed to determine the positions of the focal points as accurately as it was done for the other curves rises quickly. We did not investigate these parts of the caustic which connect to the lines ADC and RST because they do not affect the central structure of Σ_{CM} and hence the parallels with Σ_{TPM}.

Conclusions

In this study of the pure $SU(2)$ lattice gauge theory in the Hamiltonian formalism on a cube with anti-periodic boundary conditions it has been shown that the occurence of caustics as found by Bartels and Wu is not limited to the models investigated by them but obviously is a pertinent feature of the underlying theory. This is also confirmed by their recent work [8] on a large N^3 lattice. In comparison with the two-plaquette model studied by these authors the caustic in the cube model shows a far more detailed structure which may be interpreted as the first sign for the onset of a self-repetitive pattern as seen in the 'cones inside cones' described in [8], a picture which hopefully may be brought in contact with renormalization group ideas [11] and the conventional views on the behaviour of theories near a critical point. All this lends support to the expectation that caustics may contribute significantly to the vacuum structure of gauge theories.

Acknowledgements

I thank J. Bartels for many helpful discussions.

References

[1] J.Bartels and T.T.Wu,
Caustics in a Simple $SU(2)$ Lattice Gauge Theory Model,
Z. Phys. **C33** (1987) 583-603
(also published as report DESY-86-096)

[2] J.Kogut and L.Susskind,
Hamiltonian formulation of Wilson's lattice gauge theories,
Phys. Rev. **D11** (1975) 395–408

[3] M.Creutz,
Quarks, Gluons and Lattices,
Cambridge (University Press) 1983

[4] V.I. Arnold,
Mathematical Methods of Classical Mechanics,
New York (Springer, Graduate Texts in Mathematics 60) 1978

[5] L.S. Schulman,
Techniques and Application of Path Integration
New York (J. Wiley & Sons) 1981

[6] V.I. Arnold, S.M. Gusein-Zade and A.N. Varchenko,
Singularities of Differentiable Maps, Vol. I,
The Classification of Critical Points, Caustics and Wave Fronts,
Boston (Birkhäuser) 1985

[7] J.B.Bronzan,
Explicit Hamiltonian for $SU(2)$ lattice gauge theory,
Phys. Rev. **D31** (1985) 2020–2028

[8] J.Bartels and T.T.Wu,
Semiclassical Analysis of the Weak Coupling Limit of $SU(2)$ Lattice Gauge Theory: the Subspace of Constant Fields,
report DESY-87-120, to appear in Phys. Rev. **D**

[9] J. Bartels and N.K. Falck,
Path Integral on a Group Manifold and the Lattice Gauge Theory Hamiltonian,
report DESY-87-130

[10] L.Collatz,
The Numerical Treatment of Differential Equations,
Berlin (Springer) 1966, 2^{nd} pr. of 3^{rd} ed.

[11] D.F. Escande,
Stochasticity in classical Hamiltonian systems: Universal aspects,
Phys. Rep. **121** (1985) 165–261

Figure Captions

Fig. 1 The cube with anti-periodic boundary conditions.
The full lines refer to k(1), the broken lines to k(2) and the dotted lines to k(3).

Fig. 2 The potential $V(\Theta_1, \Theta_2, \vartheta_r)$ for $\vartheta_r = 0, \frac{1}{5}\pi, \ldots, \pi$

Fig. 3 At a focal point $\det(\dot{x}, \delta^1 x, \delta^2 x) = 0$

Fig. 4 The regions Γ and Γ' in the configuration space spanned by Θ_1, Θ_2 and ϑ_r

Fig. 5 The caustic of the two-plaquette model.
ABC: cusp
F : bottle neck

Fig. 6 One half of the upper part of the caustic of fig. 5 with lines of constant Θ_Δ

Fig. 7 Half of the upper part of the caustic
modified by the twist in the part approaching C

Fig. 8 Half of the upper part of the caustic in the cube model with twist and seam

Fig. 9.a Structure of half of the upper part of the caustic in the cube model
viewed along the Θ_2-axis under an angle of 45° from above;
BB': intersection of seam with plane of symmetry
F : bottle neck
FD : sharp edge
(1) : line $\Theta_\Delta = 0$, $\vartheta_r = 0$
(2) : $\Theta_\Delta = 0$, $\vartheta_r = \vartheta_r(F)$
(3) : $\Theta_\Sigma = \Theta_\Sigma(B')$, $\Theta_\Delta = 0$
(4) : $\Theta_\Sigma = \Theta_\Sigma(B')$, $\vartheta_r = 0$

Fig. 9.b Same as fig. 9.a with a net of focal points on half of the upper part of the caustic

Fig. 10.a Trajectories in the $(\Theta_\Delta = 0)$-plane forming the seam

Fig. 10.b Envelope of trajectories depicted in fig. 10.a

Fig. 11 Half of the lower part of the caustic of fig. 5 with lines of constant Θ_Δ

Fig. 12 Half of the lower part of the caustic in the cube model

Fig. 13.a Structure of half of the lower part of the caustic in the cube model
projected onto the plane of symmetry

Fig. 13.b Same as fig. 13.a with a net of focal points on one half of the lower part of the caustic

Fig. 14 Structure of one half of Σ_{CM}, the caustic formed by the first and second focal points in the cube model

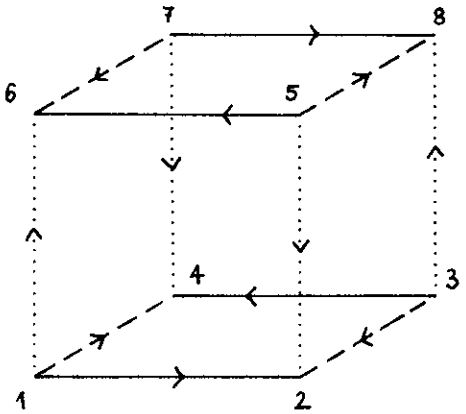

Fig. 1

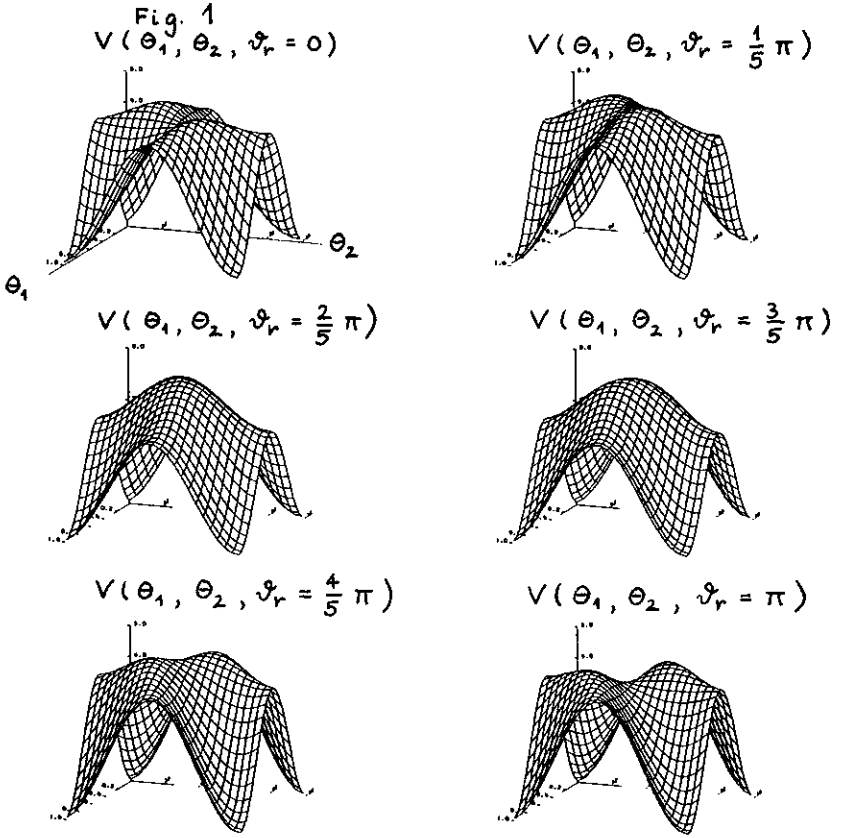

Fig. 2

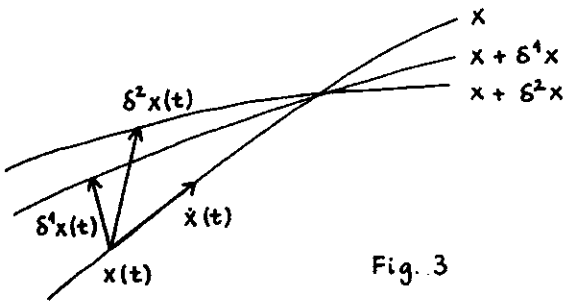

Fig. 3

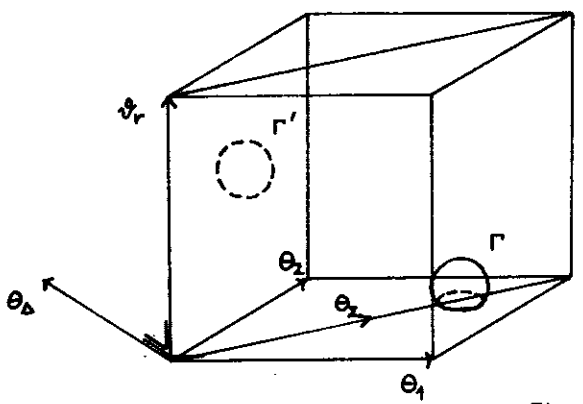

Fig. 4

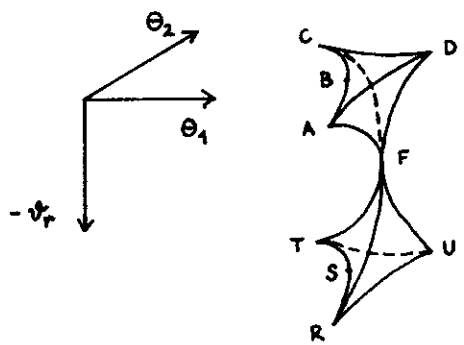

Fig. 5

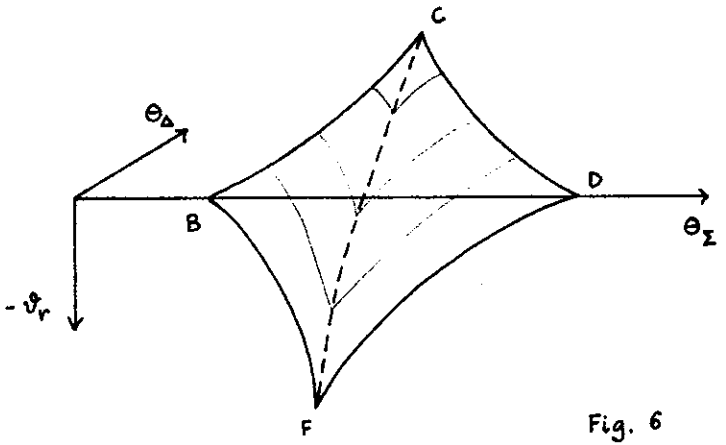

Fig. 6

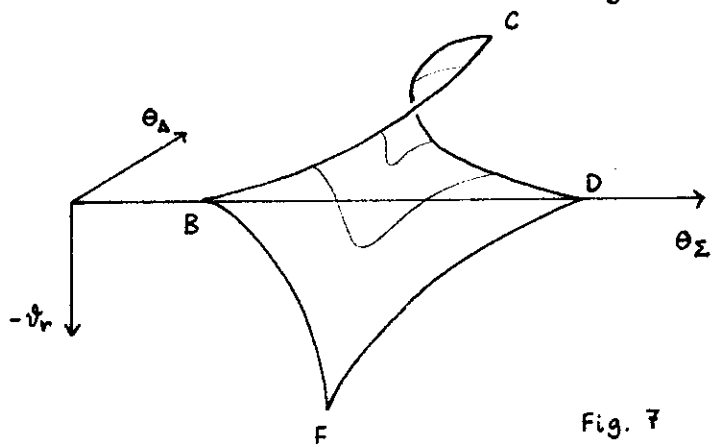

Fig. 7

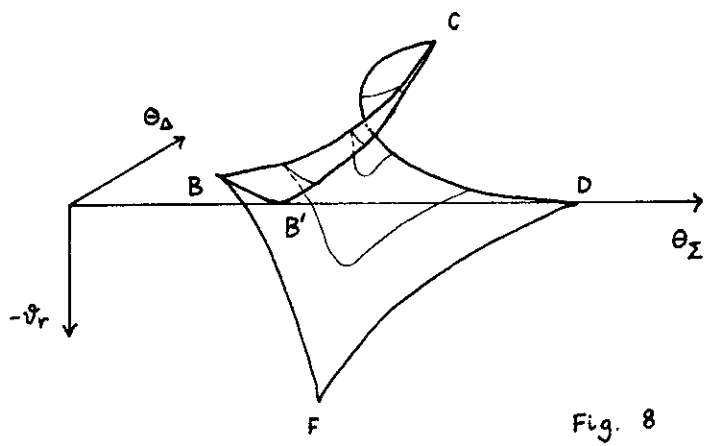

Fig. 8

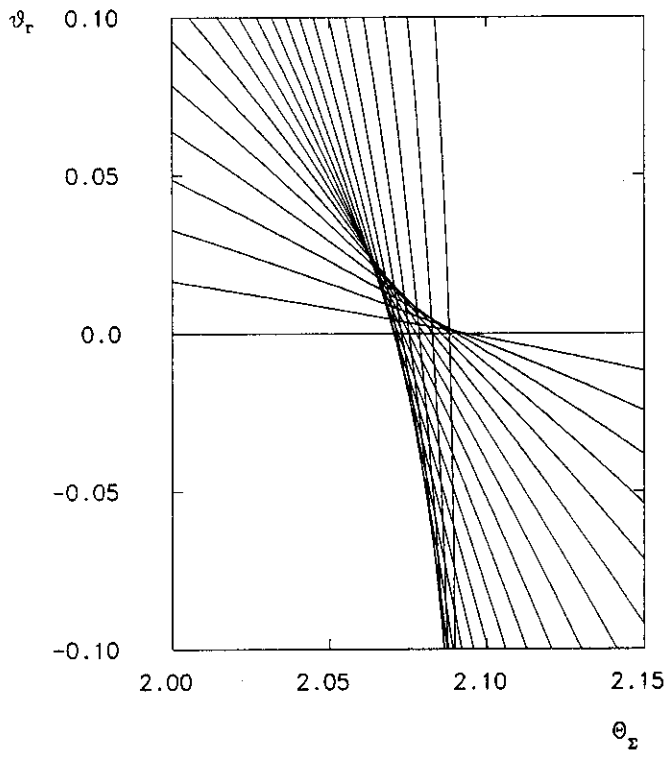

Fig. 10.a

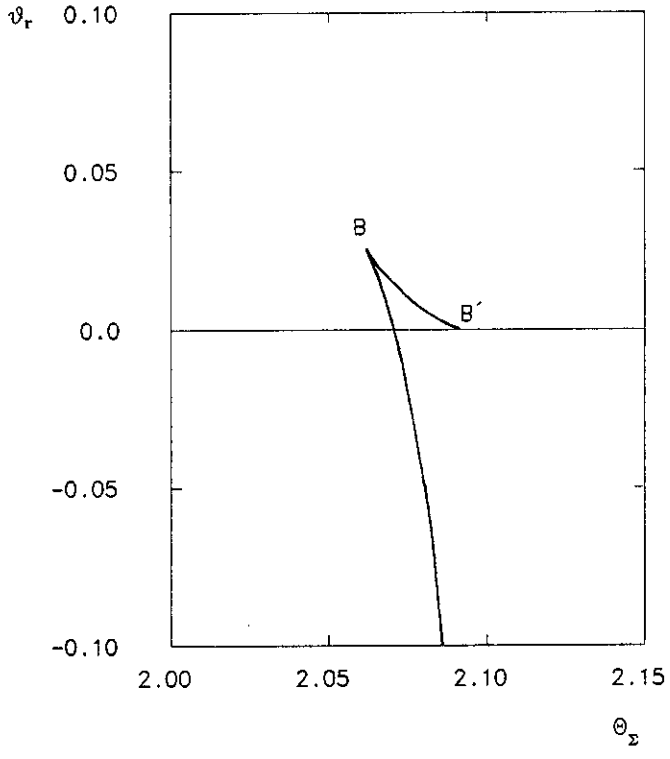

Fig. 10.b

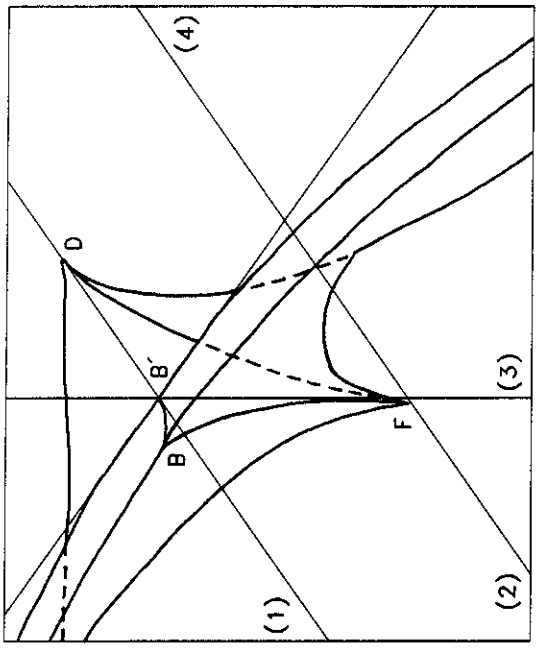

Fig. 9.a

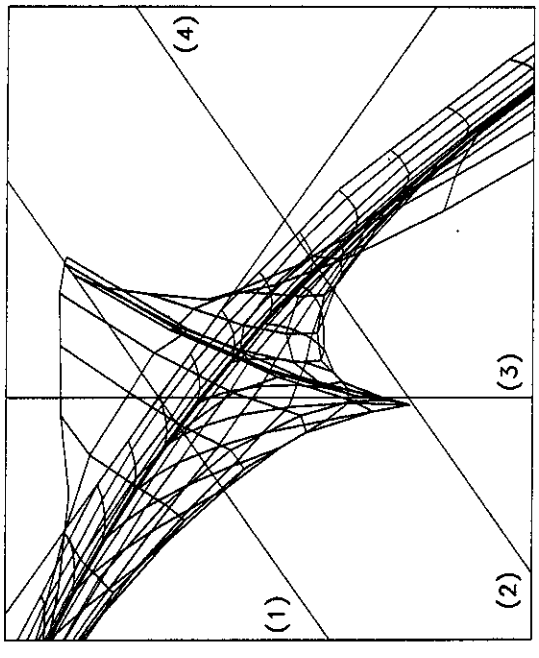

Fig. 9.b

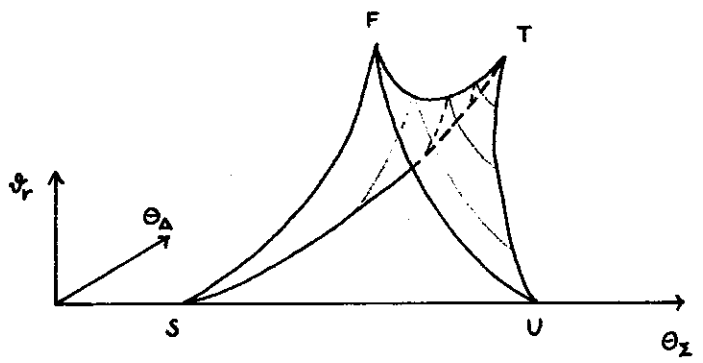

Fig. 11

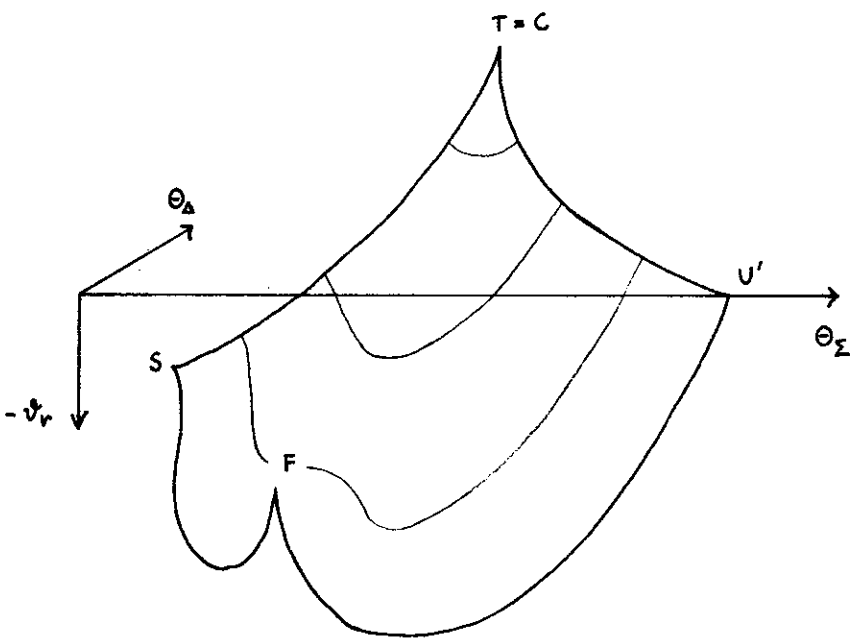

Fig. 12

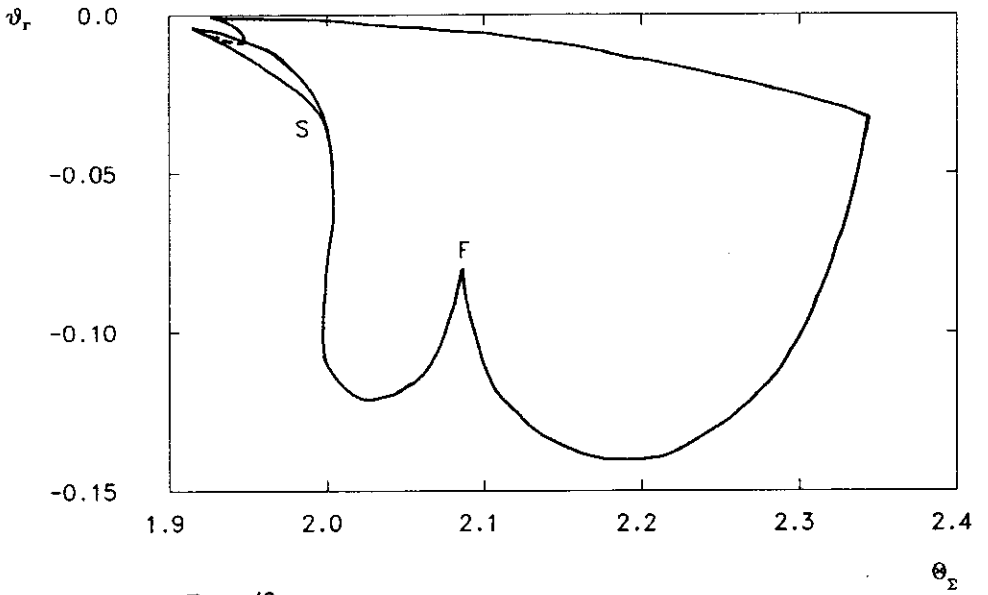

Fig. 13.a

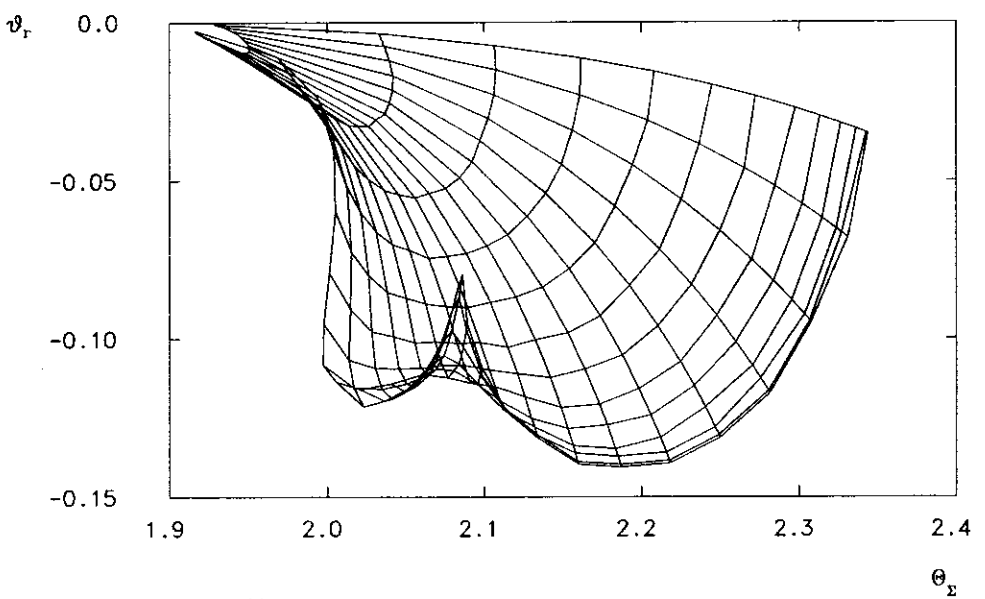

Fig. 13.b

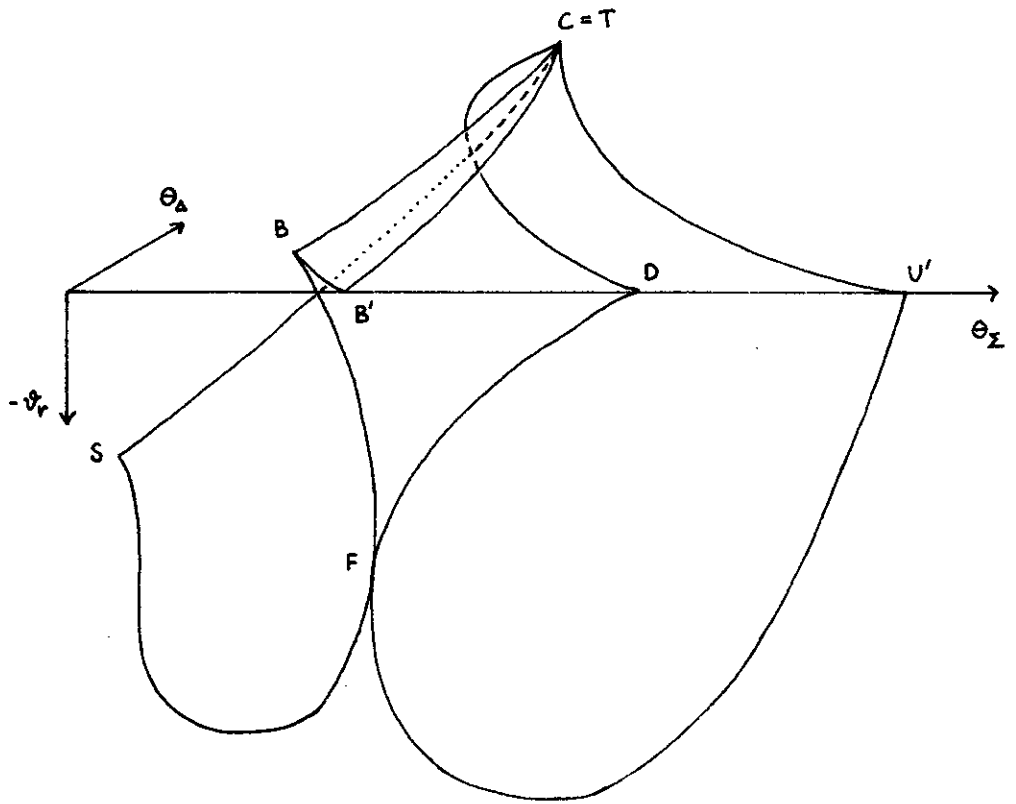

Fig. 14